Journal of Innovative Optical Health Sciences
Vol. 2, No. 1 (2009) 9–25

World Scientific
www.worldscientific.com

NON-LINEAR OPTICAL IMAGING OF OBESITY-RELATED HEALTH RISKS: REVIEW

THUC T. LE* and JI-XIN CHENG†

*Weldon School of Biomedical Engineering
Purdue University
West Lafayette, Indiana 47907, USA
thuc@purdue.edu

†Department of Chemistry and
Weldon School of Biomedical Engineering
Purdue University
West Lafayette, Indiana 47907, USA
jcheng@purdue.edu

This review highlights the recent applications of non-linear optical (NLO) microscopy to study obesity-related health risks. A strong emphasis is given to the applications of coherent anti-Stokes Raman scattering (CARS) microscopy where multiple non-linear optical imaging modalities including CARS, sum-frequency generation (SFG), and two-photon fluorescence are employed simultaneously on a single microscope platform. Specific examples on applications of NLO microscopy to study lipid-droplet biology, obesity-cancer relationship, atherosclerosis, and lipid-rich biological structures are discussed.

Keywords: Atherosclerosis; coherent anti-Stokes Raman scattering; lipid droplet; mammary cancer; non-linear optics; obesity; second harmonic generation; sum-frequency generation; two-photon fluorescence; tumor stroma.

1. Introduction

Obesity has reached an epidemic proportion in the United States and many other developed nations.[1,2] The adverse effects of obesity on major human diseases including cancer, diabetes, and cardiovascular diseases are posing significant challenges to global public health management.[1–3] Obesity is a disorder resulting from an imbalance in energy homeostasis where energy intake exceeds expenditure. When excess energy stored in the form of adipose tissues accumulates such that the body fat mass index rises above $30\,\mathrm{kg/m^2}$, an obese condition is diagnosed.[2] In addition to the lipid storage role, adipose tissues also serve as endocrine organs.[4,5] As adipose mass increases, adipocyte-secreted protein hormones, or adipokines, dominate the body physiological response and regulation.[4,6] Adipokines have been shown to adversely influence many processes including body weight homeostasis, insulin resistance, diabetes, inflammation, atherosclerosis, osteoporosis, and carcinogenesis.[2,5,6]

Currently, the investigation of obesity and its impact on other diseases relies on standard histological evaluation of tissue biopsies or biochemical profiling of metabolites.[6] While serving as powerful diagnostic tools for a number of diseases, such techniques present limitations to the study of obesity. Fixed tissues for light or electron microscopy examination prevent real-time observation of lipid absorption, metabolism, storage, and mobilization.[7]

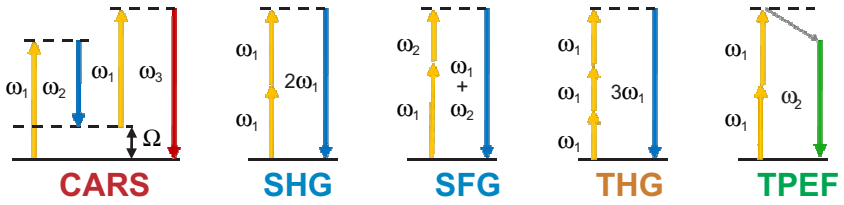

Fig. 1. Energy diagrams for NLO imaging modalities. CARS is a four-wave mixing process where molecular vibration frequency Ω is equal to $\omega_1 - \omega_2$. When Ω matches Raman-active band of CH_2 at 2840 cm^{-1}, vibrational contrast of lipid-rich structures is generated. SHG and SFG combine photons of equal energy (SHG) or of different energy (SFG) to generate new photons with combined energy. SHG and SFG are sensitive to non-centrosymmetric biological structures including collagen fiber and microtubule. THG combines photons of equal energy to form new photons with triple the energy. THG is dependent on optical heterogeneities of probed objects which include third-order non-linear susceptibility, refractive index, and refraction. Two-photon excitation fluorescence (TPEF) combines energy of two photons to excite one molecule to an excited state which subsequently proceeds along the fluorescence-emission pathway. TPEF is widely used to image fluorescently-labeled molecules.

Standard biochemical assays including Western and Northern blots describe static population average behaviors; thus, these are insufficient to study malfunctions in spatial-temporal control of dynamic cellular events which trigger the onset of the disease.[8] As a result, investigation of non-mutative causes of obesity remains inaccessible.[9–11] Furthermore, identifying specific type of lipid in tissue biopsies is not achievable using current imaging techniques. Unlike many proteins where there are specific antibodies, most lipid molecules have no known specific marker.[7] Clearly, new methodologies which allow non-invasive, real-time, compositional, and single-cell measurement of lipid are needed to advance our understanding of obesity and related diseases.

An opportunity for advancing obesity research can be found with coherent anti-Stokes Raman scattering (CARS) microscopy.[7,12,13] With intrinsic three-dimensional spatial resolution and relatively high penetration depth, CARS imaging opens up a new window for non-invasive visualization of cell morphology and function in tissues and live animals. CARS is a four-wave mixing process in which a pump field $E_p(\omega_p)$ and a Stokes field $E_s(\omega_s)$ synchronously interact with a sample to generate an anti-Stokes field E_{as} at frequency $2\omega_p - \omega_s$ (Fig. 1). Because the CARS signal is significantly enhanced when $\omega_p - \omega_s$ is tuned to a Raman-active vibration band, it allows for chemically selective imaging. Furthermore, intrinsic coherent property allows CARS signal to increase quadratically with respect to the number of molecular vibrations in the focal volume. CARS microscopy is particularly sensitive to lipid-rich structures when $\omega_p - \omega_s$ is tuned to 2840 cm^{-1} which matches the symmetric vibration of CH_2 bonds. Label-free visualization capability for lipid structures renders CARS an ideal tool for lipid research. Moreover, label-free visualization capability is highly advantageous for *in vivo* imaging where labeling can be complicated by inefficient diffusion and non-specific binding.[7]

An additional unique advantage of CARS microscopy is its intrinsic capability for multimodal non-linear optical (NLO) imaging.[13,14] A typical CARS microscope with picosecond pulse excitation is capable of simultaneous CARS, sum frequency generation (SFG), and two-photon excitation fluorescence (TPEF) imaging (Fig. 1, Table 1). TPEF microscopy has been widely used for molecular imaging due to the versatility of fluorescent molecules.[14] SFG or second harmonic generation (SHG) microscopy has been used to probe polarized proteins due to its sensitivity to non-centrosymmetric structures (Fig. 1).[15] Furthermore, SFG and CARS do not require electronic resonance, thus longer excitation wavelengths can be used which could minimize multiphoton absorption-induced photodamage and increase tissue penetration depth.[13,14] Using multimodal imaging capability of a CARS microscope, many biological structures within the tissue biopsies and live animals have been simultaneously visualized.[7]

With many apparent advantages, CARS microscopy has been widely applied to study various aspects relating to lipid storage, metabolism, and related diseases.[7,13] In the following sections, we will present reviews of current literatures on the applications of CARS microscopy to lipid research. In addition, we will discuss relevant advances in lipid research using other techniques. Specifically, we will focus this review on the applications of CARS microscopy to study: (1) lipid-droplet biology, (2) lipid metabolism in simple organisms, (3) obesity-cancer relationship,

Table 1. Comparison of NLO imaging modalities.

Imaging modality	Origin of signal	Advantage	Limitation
TPEF	Fluorescence	Versatility of fluorescent probes	Photobleaching, inefficient labeling
SFG/SHG	Lack of inversion symmetry	Label free	Limited non-centrosymmetric biological structures
THG	Optical heterogeneity	Simplicity of experimental set-up, low tissue excitation scattering	High tissue emission absorption
CARS	Molecular vibration	Chemically selective, label-free, highly sensitive for lipid-rich structures	Expensive complex experimental set-up

(4) atherosclerotic lesions, and (5) lipid-rich structures including myelin sheath, skin, and brain.

2. Lipid-Droplet Biology

As energy storage depots, adipose tissues play crucial roles in the regulation of energy homeostasis.[4] In animals, as in humans, increased and decreased adiposity in times of nutritional abundance and famine are observed, respectively. Under normal physiological conditions, adipose tissues serve as highly dynamic organs whose functions include storing or dispensing energy according to the energy demand of the body.[4] However, perturbations including genetic adaptations have been shown to disrupt the regulation of energy homeostasis.[3,4] A typical example of such perturbations can be found in Ossabaw swine of Ossabaw Island, Georgia.[16] Abandoned by Spanish explorers more than 500 years ago, Ossabaw swine evolved an adaptive genetic mutation in the AMP-activated kinase gene which allows it to store massive amount of fat during time of abundance and survive during long periods of famine.[16,17] While such a genotype favors the survival of Ossabaw swine on the island where living conditions are harsh, it is the cause of obesity, diabetes, and cardiovascular diseases in domesticated Ossabaw swine when food is plentiful and exercise is scarce.[16] Similar occurrences have been observed in many human ethnic groups where the convenience and nutritional abundance of modern living are strongly associated with the steady rise in severe obesity and diabetes conditions over last century.[3] Nonetheless, the cause for obesity in human beings remains less clearly understood.

To study the cause of obesity, significant research efforts have focused on lipid-droplet biology of fat cells or adipocytes.[4,18] An *in vitro* cell culture model was developed by Green and Kehinde[19] in 1974 to study the differentiation of 3T3-L1 cells into adipocytes. Using this model system, transcriptional regulation of adipocyte differentiation has been extensively studied.[18] In-depth knowledge of adipocyte differentiation has been thoroughly discussed in many recent reviews.[4,18] In general, adipocyte differentiation has been measured in terms of adipogenic genes expression and intracellular lipid droplets (LDs) accumulation. The commitment to differentiation is indicated by the activation of a nuclear transcription factor, PPARγ, which controls the expression of terminally differentiated genes including genes encoding for lipid synthesis enzymes.[18] And the degree of differentiation is indicated by the quantity of intracellular LDs. However, current measurement techniques are inadequate to describe the dynamic nature of lipid metabolism within adipocytes. Adipogenic gene expression profiling using Northern blots or real-time PCR provides average population measurements of extracted mRNA transcripts. And the measurement of LDs, which relies on oil red O (ORO) or red Nile staining of fixed cells, provides static snapshots of the intracellular lipid pool. Such static measurements are insufficient to investigate the dynamic control of LDs mobilization during increased cellular energy demand. As a result, the dynamic process including lipolysis remains understudied. Furthermore, population measurements hinder the investigation of cell-to-cell variability during drug-induced differentiation of 3T3-L1 cells.[20] Consequently, heterogeneity in drug response of adipocytes remains a well-observed but poorly understood phenomenon.[19] Such drug-response heterogeneity poses significant challenges to the evaluation of drugs aiming at interfering with fat cell differentiation.[20]

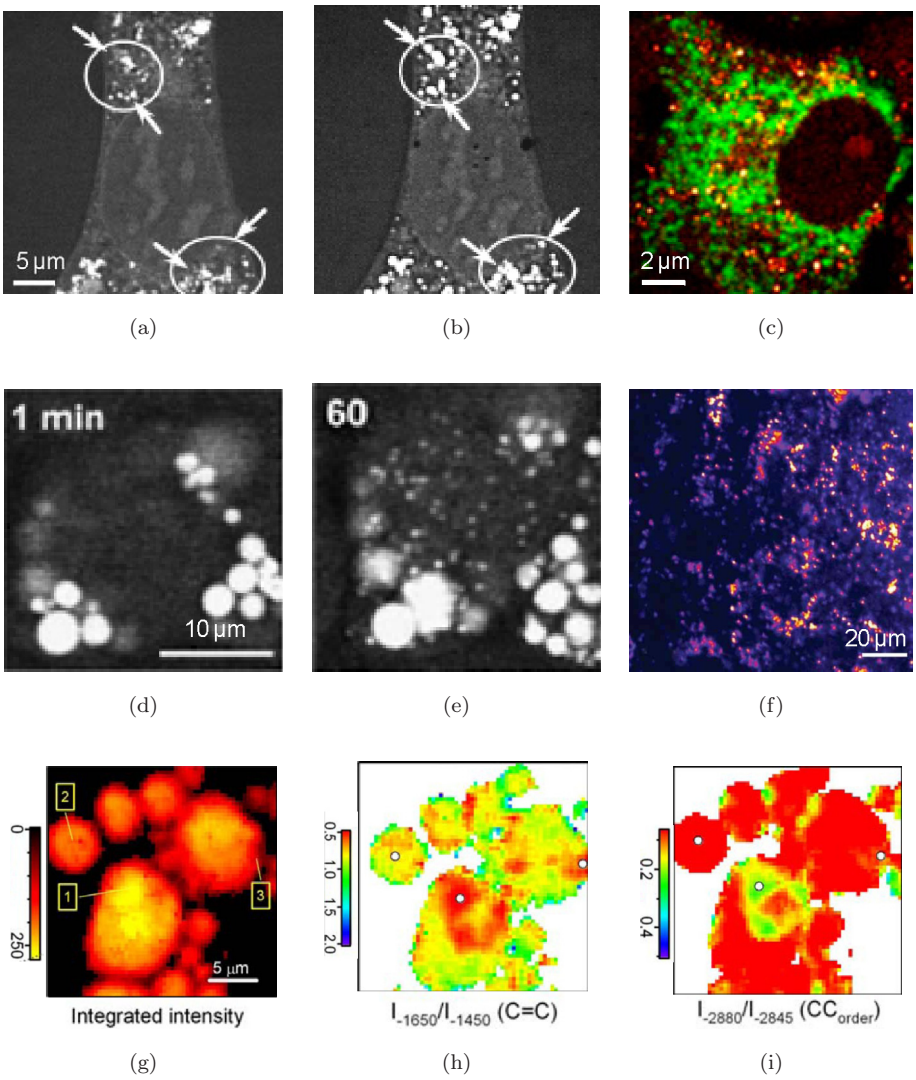

(a) (b) (c)

(d) (e) (f)

(g) (h) (i)

Fig. 2. The CARS and THG imaging of LDs. (a) and (b) Evidence of ORO staining induced LD fusion in fixed 3T3-L1 cells. (a) 5 min and (b) 15 min after ORO addition. (c) CARS imaging of LDs and TPEF imaging of labeled mitochondria in adrenal cortical Y-1 cells. (d) and (e) CARS imaging of LD lipolysis at 1 min (d) and 60 min (e) after lipolysis stimulation. (f) THG imaging of a liver tissue. (g) to (i) Multiplex CARS spectral imaging of LD composition and packing within a single 3T3-L1 cell. (g) Integrated intensity of LDs. Mapping the degree of unsaturation (h) and acyl chain order, and (i) within LDs. Images reproduced from Nan *et al.*, Yamguchi *et al.*, Debarre *et al.*, and Rinia *et al.* with permission.

Using CARS microscopy, the dynamics of lipid droplets synthesis and transport have been monitored in live cells. Taking advantage of the label-free imaging capability of a CARS microscope, Nan *et al.*[21] described the dynamics of lipid synthesis in live 3T3-L1 cells over time.[4] After the addition of adipogenic stimulants, the CARS imaging showed an initial clearance of small LDs followed by an eventual accumulation of large LDs. The CARS imaging of unstained LDs was nonperturbative; whereas, the fluorescent imaging of ORO and red Nile stained LDs required cell fixation. Moreover, ORO staining induced LDs aggregations and perturbed LD structures (Figs. 2(a) and (b)).[21]

CARS imaging also allowed Nan *et al.*[21] to track lipid-droplet transport in adrenal cortical Y-1 cells. Simultaneous CARS imaging of LDs and TPEF of stained mitochondria revealed possible interaction between LDs and cellular organelle (Fig. 2(c)).[22] Taken together, Nan *et al.* demonstrated the possible applications of CARS microscopy to monitor LDs in living cells.

Furthermore, CARS microscopy has been applied to study lipolysis of LDs in living cells. Yamaguchi *et al.*[23] combined CARS imaging of LDs with standard molecular biology techniques to mechanistically elucidate the role of a LD surface protein, CGI-58, in lipolysis. Using RNA

interference (RNAi) to knock down CGI-58 gene did not interfere with adipocyte differentiation. However, excess LD accumulation and reduced lipolysis activity were observed. By itself, CGI-58 did not exhibit lipase activity, but its expression enhanced the activity of adipose triglyceride lipase. CGI-58 interacts with perilipin, another LD surface protein critical for lipolysis in adipocytes. Phosphorylation of perilipin disrupts interaction with CGI-58 leading to a dispersal of CGI-58 away from LDs and into cytoplasm. The CARS imaging of micro-LDs formation during lipolysis in CGI-58 knock-down cells revealed that CGI-58 was not required for micro-LDs formation. Yamaguchi *et al.* concluded that CGI-58 plays a role in LD lipolysis in cooperation with perilipin and lipases. Yamaguchi *et al.* demonstrated a limited role of CARS microscopy in the functional studies of CGI-58 where it was primarily used to image the vesiculation of micro-LDs from large LDs upon hormonal stimulation (Figs. 2(d) and (e)). Nonetheless, future CARS application to the studies of LDs dynamics should bring new understanding on a significant but understudied field of LD biology.[24]

In addition to CARS microscopy, the third harmonic generation (THG) microscopy has recently been demonstrated to be a non-perturbative imaging method for LDs.[25] The THG signal generation mechanism is highly dependent on optical heterogeneities of objects in the probed medium which include third-order non-linear susceptibility, refractive index, and refractive index refraction. Because the optical properties of lipid and water are highly different from one another, LDs in aqueous environment of cell cytoplasm generate strong optical contrast with THG imaging. Debarre *et al.*[25] successfully applied THG to visualize LDs in hepatocytes, insect embryos, plant seeds, and intact rat lung tissues (Fig. 2(f)). The THG signals emanating from LDs were 20 to 100 folds higher than other cellular components. Thus, Debarre *et al.*[25] argued that THG could be an alternative to CARS for LDs imaging.

While THG has undoubtedly proven to be a powerful imaging method for LDs, several limitations intrinsic to THG could render it less attractive than CARS for lipid research. First, THG does not have chemical selectivity, which is an intrinsic property to CARS microscopy.[12,25] This drawback limits the capability of THG in visualizing LDs and tracking LDs movement. THG cannot distinguish the composition of one LD from another. On the contrary, CARS signals arise from molecular vibration, thus CARS can resolve different chemical bonds in the same focal volume. Cheng *et al.*[26] employed multiplex CARS to resolve symmetric and asymmetric $-CH_2$ and $-CH_3$ stretch vibration in a lipid vesicle. Muller and Schins[27] employed multiplex CARS to distinguish liquid from gel phase of a lipid membrane based on hydration and saturation degree of lipid. Li *et al.* sequentially and Burkacky *et al.* simultaneously resolved lipid species based on the difference in molecular vibration of $-CD_2$ at 2100 cm^{-1} from $-CH_2$ at 2845 cm^{-1}.[28,29] Most recently, Rinia *et al.*[30] resolved the composition and packing of LDs using multiplex CARS microscopy (Figs. 2(g) to (i)). Thus, CARS provides composition information not accessible by THG. Second, THG strong signals from LDs would be significantly diminished in thick tissue environment. THG signals induced with ∼1200 nm pulse laser excitation would emit photons at ∼400 nm which falls into the absorption region of many tissue components including vasculature and blood cells. Consequently, THG emission photons would fail to escape thick tissues, thus, reducing the THG detection sensitivity. Currently, THG has not been applied for LDs imaging in complex tissue environments or in living animals.[25] On the other hand, CARS has been widely applied to image adipocytes, lipid-rich sebaceous glands, and axonal myelin sheaths in living animals with high sensitivity and with penetration depth of up to 130 μm.[31,32] With such apparent advantages, CARS microscopy would continue to be an attractive method for lipid research.

Nonetheless, CARS imaging of LDs should be combined with the analysis of other cellular processes to advance LD biology research. Using genome-wide RNAi screen in *Drosophila* S2 cells, Guo *et al.*[33] identified genes encoding for enzymes of phospholipid biosynthesis which determine the LDs size and number. This observation suggests that phospholipid composition affects LD morphology and utilization. With the capacity to analyze lipid composition, CARS imaging would complement genetic studies to provide in-depth functional analysis of the relationship between genotype and LD phenotypic expression. In addition, a wide range of fluorescent gene activity and kinase activity reporter systems have recently been made available.[34,35] Advances in imaging and spectroscopy techniques have also

enabled the analysis of protein-DNA, protein-RNA, and protein-protein interaction in living cells.[36−39] Combining label-free lipid imaging capability of CARS microscopy with the versatility of fluorescent reporter and analysis systems, LD biology can be investigated in real-time at the level of a single cell. Such capability would provide dynamic information not accessible by population measurements. Single-cell studies would also circumvent intrinsic cell-to-cell variability and allow direct evaluation of drug effect in adipocyte differentiation.[20] Most importantly, a number of lipid-associated proteins, whose functions are critical for LD formation and mobilization, have been identified and characterized in recent years.[24,40] Real-time and nonperturbative CARS imaging of LDs and TPEF imaging of lipid-associated protein fused to fluorescent proteins would allow spatio-temporal studies of LD-protein interaction to provide in-depth understanding of LD dynamics.

Moreover, to maximize the impact of CARS imaging on LD biology, adipogenesis should be studied in living animals. Taking advantage of high penetration depth intrinsic to TPEF imaging, Fukumura *et al.*[41] studied angiogenesis during adipocyte differentiation *in vivo* using implanted 3T3-F442A cells. However, without the capability to visualize LDs *in vivo*, Fukumura *et al.* turned to ORO staining of LDs in 3T3-F442A cell cultures to complement their observation of angiogenesis *in vivo*. The employment of CARS for *in vivo* imaging would allow visualization of adipocyte differentiation in native environments. Using multimodal imaging capability of a typical CARS microscope, multiple biological processes could be visualized simultaneously. On the same microscope platform, angiogenesis could be monitored using TPEF imaging of dye-labeled vasculatures,[42] extracellular matrix remodeling could be monitored using SHG imaging of collagen fibrils,[43] and adipocyte differentiation could be monitored using CARS imaging of LDs formation. CARS imaging of adipogenesis *in vivo* would provide a rapid means to validate the existing understanding of LD biology as well as provide new opportunity to study LD biology in native environments.

3. Lipid Metabolism in Simple Organisms

The ability to store energy in the form of cytoplasmic LDs is observed from simple organisms such as *Saccharomyces cerevisiae* to complex organisms such as humans.[40,44] In addition, there is a remarkable gene sequence and function conservation of many proteins involved in lipid synthesis and storage pathways.[44] Due to such conservation, studies of lipid metabolism in simple organisms can provide insights into the same process in complex organisms. Indeed, *Drosophila melanogaster*, *Caenorhabditis elegans*, and zebrafish have been proven to be ideal models for developmental studies due to their rapid breeding, easy maintenance, and highly amenable genetics.[45−47] In recent years, these simple organisms have been employed as models for *in vivo* NLO imaging due to their intrinsic optical accessibility.[36,48,49] It is conceivable that their employment for real-time *in vivo* imaging of gene and protein network interaction, cell-cell communication, or genotype-phenotype relationship will increase exponentially in the near future.

The first CARS applications to lipid metabolism studies in simple organisms were demonstrated by Burkacky *et al.* and Hellerer *et al.* on *C. elegans*.[29,49] Burkacky *et al.*[29] employed dual-CARS to simultaneously image symmetric CH_2 vibration at $2845\,cm^{-1}$ and CD_2 vibration at $2115\,cm^{-1}$ of LD in *C. elegans* which allowed removal of nonresonance background and improvement in image sensitivity and contrast. Hellerer *et al.*[49] used CARS imaging to screen how genetic variations in lipid metabolism pathway influence size, distribution, and lipid order state of LDs during development of *C. elegans* larvae (Fig. 3). In addition to LDs visualization, Hellerer *et al.* simultaneously monitored symmetric CH_2 vibration at $2845\,cm^{-1}$ and asymmetric CH_2 vibration at $2880\ cm^{-1}$ (Fig. 3(a)). A high ratio of asymmetric to symmetric CH_2 vibration is associated with gel phase. LDs storage in early-stage and late-stage larvae development had low and high ratio of asymmetric to symmetric CH_2 vibration, respectively. This observation suggests a transition from liquid phase to gel phase of LDs with age. Conversely, the promotion of lipid storage in a genetic mutant was associated with a shift from gel phase to liquid phase. By monitoring changes in lipid phase (Fig. 3(a)) and the abundance of LDs (Figs. 3(b) and (c)), Hellerer *et al.* argued that the state of lipid metabolism of *C. elegans* can be inferred. These initial works demonstrated that combining CARS imaging with optically accessible *C. elegans* could provide a rapid platform for *in vivo* studies of the mechanisms underlying obesity and metabolic diseases.

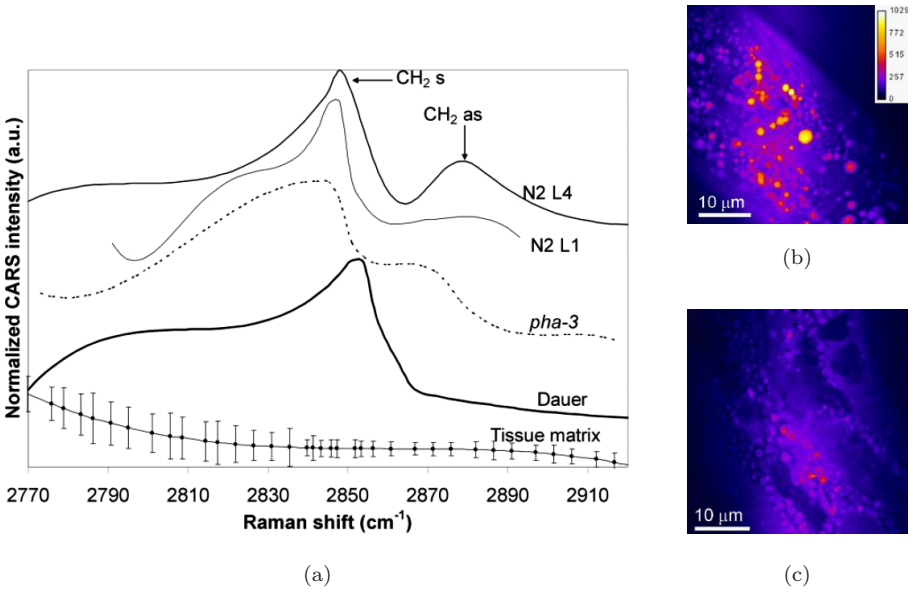

(a) (b) (c)

Fig. 3. CARS imaging of lipid metabolism in *Caenorhabditis elegans*. (a) CARS spectra of LDs in wild type and mutant *C. elegans*. Symmetric and asymmetric CH_2 peaks at 2845 cm^{-1} and 2880 cm^{-1}, respectively. N1 L1 and N1 L4 represent wild type at early and late larvae stage, respectively. Mutant *pha-3* has a feeding-defective phenotype. Mutant *daf-4* dauer has deficiencies in insulin and TGF-β signaling pathway. Tissue matrix spectrum indicates sampling frequency and standard deviation. CARS images of wild type (b) and *pha-3* mutant (c) show reduced LDs accumulation in feeding-defective nematode. Images reproduced from Hellerer *et al.* with permission.

4. Impact of Obesity on Mammary Tumor Stroma

Obesity is an established risk factor for many types of cancer including colon, breast, endometrium, kidney, esophagus, pancreas, gallbladder, and liver.[1] However, significant bodies of current literature on the relationship between obesity and cancer development are focused on breast cancer due to the microenvironment rich in adipocytes surrounding mammary epithelial cells.[50] Systematic studies of the impact of adipokines on malignant breast ductal epithelial cells showed that adipokines promote tumorigenesis by inducing the expression of genes regulating cancer cell proliferation, invasion, survival, and angiogenesis.[51,52] In addition, adipokines increased the activity of pro-oncogenic factors including β-catenin and CDK6 by reducing the expression of their inhibitors.[51] Nonetheless, tumor development is dependent not only on intrinsic factors such as gene mutation or activation of pro-oncogenes but also on extrinsic factors including extracellular matrix remodeling and stromal cells interaction.[53,54] Indeed, a number of stromal cells have been shown to assist tumor cell escape into bloodstream including fibroblasts, macrophages, and mesenchymal stem cells.[55–57] Rearrangement of collagen fibrils around tumor mass has been shown to facilitate tumor invasion into neighboring tissues.[58] Furthermore, extensive angiogenesis has been observed in primary and metastasized tumors to supply nutrients to the growing colonies.[59,60]

In recent years, our laboratory has employed multimodal imaging capability of a CARS microscope to evaluate the impact of obesity on mammary tumor stroma.[61] To describe the effects of obesity on the composition and 3D architecture of mammary tumor stroma, we imaged tissue biopsies of a Sprague-Dawley rat model. A unique feature of this animal model is that lean and obese rats exhibit predictable methylnitrosourea-induced tumorigenesis in benign and aggressive mammary tumors, respectively.[62] Thus, the difference in tumor stromal architecture and composition can be directly correlated to tumor grades. Simultaneous CARS and SHG imaging revealed significant tumor and stromal components including mammary adipocytes, blood capillaries, collagen fibrils, and tumor cells which can be visualized without labeling (Figs. 4(a)–(c)).[61] Expectedly, the adipocytes of obese rat mammary gland exhibited LDs with an average diameter of approximately

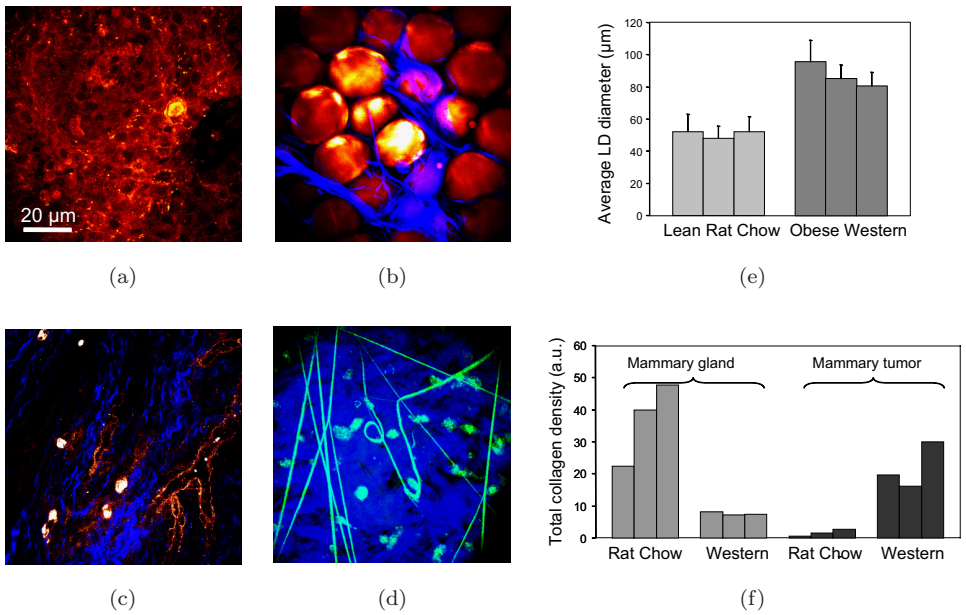

Fig. 4. The NLO imaging of mammary tumor stromal composition. (a) CARS imaging of mammary tumor cells. (b) CARS (orange) imaging of mammary adipocytes and SHG (blue) imaging of collagen fibrils. (c) CARS (orange) imaging of mammary blood vessels and SHG (blue) imaging of collagen fibrils. (d) TPEF (green) imaging of FITC-IB4-labeled microvessels and macrophages and SHG (blue) imaging of collagen fibrils. (e) Average LD diameter of adipocytes of 3 lean and 3 obese mammary glands. Error bars represent distribution of LD diameters. (f) Total collagen density, as determined by SHG signal intensity, of mammary glands and tumor stroma of lean and obese Sprague-Dawley rats. Lean and obese rats were fed with Rat Chow and Western diet, respectively. Samples from three rats of each diet group were analyzed. Images adapted from Le *et al.*

2 folds higher than those of lean rat mammary gland (Fig. 4(e)). Correspondingly, stromal collagen fibril density was higher in obese rats with aggressive tumors as compared to lean rats with benign tumors (Fig. 4(f)). Thus, a correlation between obesity and cancer aggressiveness was observed based on increased collagen density of tumor stromal extracellular matrix. Independent studies by Provenzano *et al.*[63] also associate increased collagen fibrils with cancer aggressiveness.

Most significantly, CARS microscopy is an ideal imaging tool to study the impact of obesity on tumor stromal organization and remodeling due to its ability for 3D visualization of significant tumor components. CARS and SHG imaging revealed collagen fibrils wrapping around blood vessels in tumor stroma (Figs. 5(a)–(c)). This observation supports a proposed role of collagen fibrils in guiding and promoting angiogenesis.[64] Thus, increased collagen density in obese tumor stroma could potentially support increased angiogenesis. Additionally, CARS imaging of cancer cells and SHG imaging of collagen fibrils surrounding tumors allowed the identification and location of the boundary of tumors (Figs. 5(d)–(f)).[61,65] Combining label-free imaging capability of CARS and SHG with fluorescent imaging of TPEF, antibodies-labeled macrophages in tumor stroma can also be identified (Fig. 4(d)).[61,66] Macrophages have been shown to be present in significant number in obese adipose tissues.[67] Moreover, the escape of the macrophage-assisted tumor into the bloodstream has been well documented.[57] Together, multimodal imaging capability of a CARS microscope is well suited for the investigation of how obesity perturbs tumor-stromal interaction in mammary cancer.

As endocrine organs, adipose tissues are likely to exert influence on distant tumor sites through the action of secreted adipokines and free fatty acids.[5,6,68,69] Indeed, an adipocyte-derived hormone, leptin, has been shown to promote tumor growth in a number of cancer types including prostate and endometrial cancer.[70] In addition, many cancer types exhibited lipid-rich phenotypes including brain, adrenal, lung, and mammary cancer.[71–73] In mammary cancer, lipid-rich carcinoma is associated with early death and aggressive clinical behaviors.[71] Despite such well-observed lipid-rich phenotypes, the role of lipid in cancer development remains poorly understood. Being highly sensitive to lipid, CARS microscopy would be an ideal tool to investigate the negative

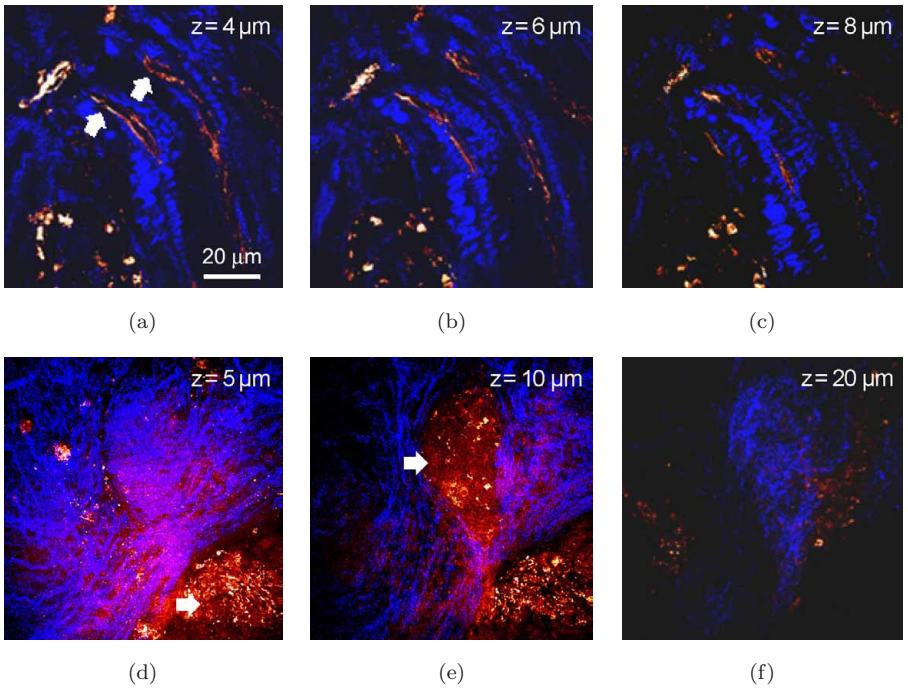

Fig. 5. The NLO imaging of mammary tumor stromal organization. (a)–(c) CARS (orange) imaging of blood vessels and SHG (blue) imaging of collagen fibrils along the vertical z axis. Arrows point to the representative blood vessels. Depth imaging reveals evidence of collagen fibrils wrapping around blood vessels. (d)–(f) CARS (orange) imaging of tumor mass and SHG (blue) imaging of collagen fibrils along the vertical z axis. Arrows point to 2 tumor areas. Depth imaging reveals the lack of collagen fibrils within the tumor mass. $z = 0\,\mu$m represents the interface of mammary tumor tissues and glass surface. Images adapted from Le *et al.*

impact of obesity on cancer development. Furthermore, recent advances in other optical imaging modalities including optical coherent tomography (OCT) and diffuse optical imaging demonstrate successes in cancer detection.[74–76] Translational development of a multifunctional endoscope which allows multimodal imaging capability would significantly enhance clinical cancer detection, diagnosis, and evaluation of tumor-stromal interaction in response to drug or nutritional intervention.

5. Composition Analysis of Atherosclerotic Plaques

Obesity and diabetes are major risk factors for cardiovascular diseases.[2,3] Approximately 16 million Americans are having pre-diabetic conditions, such as increased blood glucose, high blood cholesterol and triglycerides, and high blood pressure.[3] When these conditions are prolonged, diabetes type 2 will eventually develop. The incidence of cardiovascular diseases in diabetic individuals is four times higher than those without diabetes.[3] In 2003, cardiovascular diseases accounted for 37% of all deaths in the United States. The direct and indirect treatment cost for cardiovascular diseases was estimated to exceed US$400 billion in 2008.[77] As the trend of childhood obesity and diabetes is on the rise, the negative impact on cardiovascular diseases will be a major public health concern in the near future.

Cardiovascular diseases such as stroke, myocardial infarction, and ischemia are commonly perceived as aging diseases.[78–80] However, the process leading to such catastrophic events takes place very early in life and progressively develops over time.[79] Symptoms of cardiovascular diseases are associated with hypercholesterolemia, high blood cholesterol level, and atherosclerosis or build-up of plaques in the arterial walls.[81,82] Familial hypercholesterolemia is observed in patients as early as 5-years old and atherosclerotic lesions are detected in post-mortem autopsies as early as the second decade of life.[79,81] Early stage of atherosclerosis is initiated by the deposition of low density lipoprotein (LDL), infiltration of monocytes, and maturation of monocytes into macrophages in the intima.[82] Then, smooth muscle cells infiltrate the intima and collagen fibrils and lipid particles begin to deposit in the extracellular matrix. Advanced stage of atherosclerosis is associated with lipid-rich necrotic cores and calcium deposits in the thickened

intima. Clinical manifestation of atherosclerosis comes from plaque rupture and thrombosis which could lead to myocardial infarction and stroke.[82] Previous histological examination of tissue biopsies showed that plaque stability is dependent on its composition which includes foam cells, collagen fibrils, extracellular lipid particles, and others.[83]

Current clinical evaluation of atherosclerotic plaques are performed using non-invasive techniques such as magnetic resonance imaging and X-ray angiography, or invasive techniques such as intravenous ultrasound (IVUS) and (OCT).[84] Although these techniques provide useful cross-sectional mapping of plaque morphology and thickness, they lack both resolution and specificity necessary to analyze plaque structural organization and composition. The progression of atherosclerosis is both complex and lengthy.[82] However, current imaging technologies are only capable of detecting advanced-stage lesions.[84] Thus, early detection and prevention of atherosclerosis remains an attractive yet unrealized opportunity.

In recent years, optical imaging of atherosclerotic plaques emerges as a viable means for early-stage lesion detection and composition analysis. Optical spectroscopy techniques including fluorescence spectroscopy, Raman spectroscopy, and laser speckle spectroscopy have been used to describe composition changes associated with atherogenesis.[85–87] Most notably, Motz *et al.*[86] applied real-time *in vivo* Raman spectroscopy to identify vulnerable plaques in human with high sensitivity and specificity. Additionally, linear and NLO imaging has been employed to visualize significant components of arterial walls and atherosclerotic plaques in tissue biopsies and in living small animals.[15,88–92] Eriksson *et al.*[88] and Huo *et al.*[89] employed wide-field fluorescence imaging to study blood components-vessel walls interaction during atherogenesis in living mice. Yu *et al.*[91] and van Zandvoort *et al.*[92] employed NLO imaging to describe the composition of labeled components of vascular walls and atherosclerotic plaques in living mice. NLO imaging has several intrinsic advantages over linear optical imaging including 3D resolution, deep-tissue penetration, and SHG visualization of collagen fibrils.[14] Given such advantages, NLO imaging of tissues and animals is becoming an increasingly favored option.

Furthermore, our laboratory has recently demonstrated the capability of multimodal NLO imaging on a CARS microscope platform for label-free imaging of vascular wall and plaque composition.[93,94] Using multimodal NLO imaging, we examined arterial tissue biopsies of Ossabaw swine bearing metabolic syndrome-induced atherosclerotic plaques. CARS imaging allowed label-free visualization of smooth muscle cells, endothelial cells, foam cells, and extracellular LDs deposit based on vibrational contrast of CH_2 at 2845 cm^{-1} of lipid-rich cell membrane and LDs (Figs. 6(a)–(f)).[93] TPEF imaging allowed label-free visualization of elastin fibers of arterial walls, smooth muscle cells, and oxidized low density lipoproteins (LDL) within foam cells due to their intrinsic autofluorescence (Fig. 6(d)–(f)).[93] Additionally, SHG allows label-free visualization of collagen fibrils of both arterial walls and plaques due to its sensitivity to non-centrosymmetric structures (Figs. 6(d)–(h)).[90]

Most importantly, combined CARS, TPEF, and SHG imaging enable unprecedented analysis of both composition and organization of arterial walls and plaques.[93,94] First, multimodal NLO imaging of plaque increases accuracy of plaque detection. SHG imaging of collagen fibrils orientation showed that a plaque region where collagen fibrils appear disorganized can be distinguished from an unaffected arterial wall where collagen fibrils are organized into highly ordered and parallel fashion (Figs. 6(d)–(h)). Simultaneous TPEF and SHG imaging of healthy arterial wall revealed an appearance of TPEF signal from internal elastic lamina first, then SHG signal from arterial collagen fibrils (Fig. 6(d)); whereas, TPEF and SHG signals appeared together in the plaque due to the presence of smooth muscle cells, oxidized LDL, and collagen fibrils (Figs. 6(e), (f)). CARS imaging is highly sensitive to plaque region due to strong signals arising from extracellular LD deposits and lipid-rich foam cells (Figs. 6(c), (i)). Thus, combined CARS, TPEF, and SHG imaging would allow identification of plaque with high degree of certainty. Second, simultaneous CARS and SHG imaging of plaques revealed an inverse relationship between the number of foam cells and collagen density. Previous histological analysis associated plaque instability with thin fibrous cap, increased extracellular LDs, and increased foam cells. Thus, simultaneous CARS or TPEF and SHG imaging would allow identification of vulnerable plaques (Fig. 6(f)). Third, a primary function of macrophage in atherosclerotic lesions is to

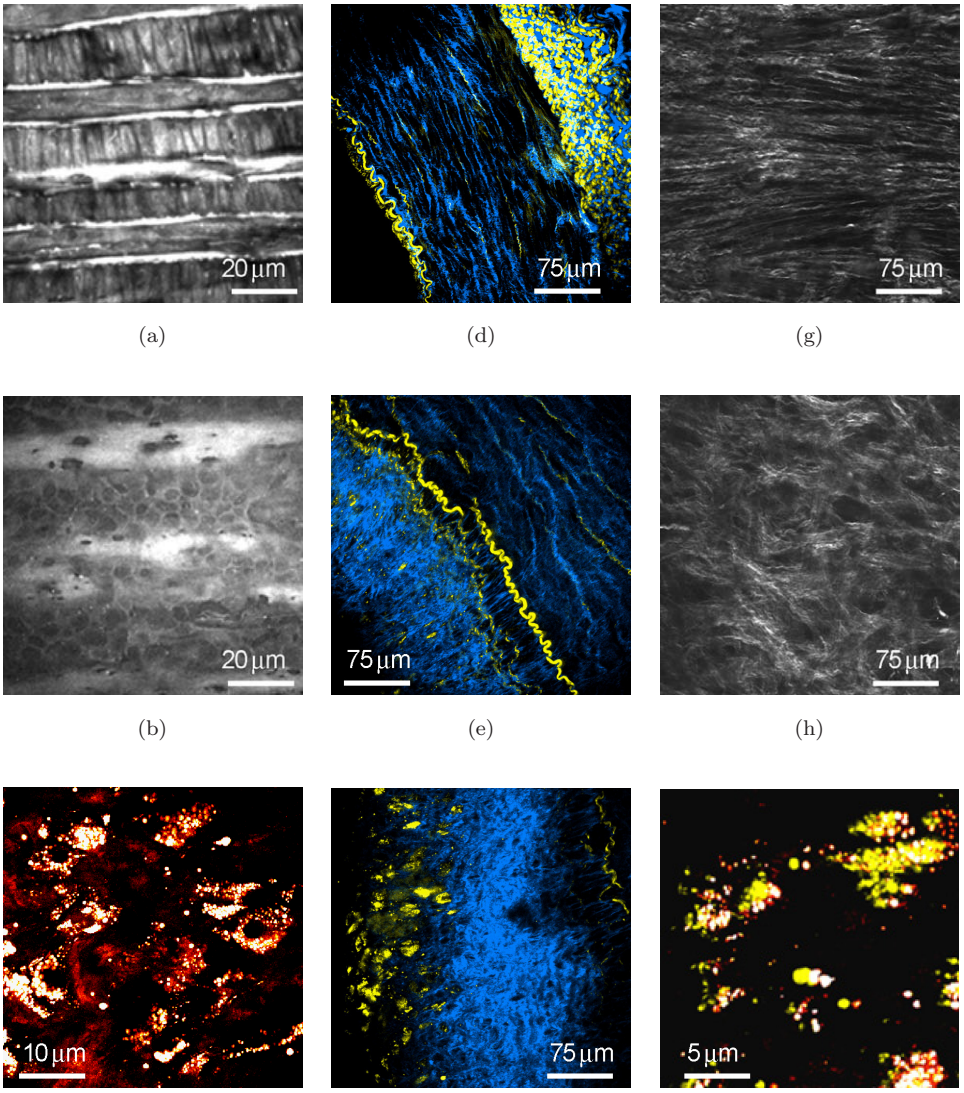

Fig. 6. NLO imaging of atherosclerotic lesion's composition and organization. Luminal CARS imaging of (a) vascular smooth muscle cells, (b) vascular endothelial cells, and (c) lipid-rich foam cells. (d) Cross-sectional SHG (blue) imaging of collagen fibrils and TPEF (yellow) imaging of elastin fibers of a normal iliac artery. (e) Cross-sectional SHG (blue) and TPEF (yellow) imaging of an atherosclerotic lesion. Plaque components extended into the lumen beyond an interrupted internal elastic lamina. (f) TPEF (yellow) signals arise from both elastin fiber and lipid-rich foam cells. Luminal SHG imaging of collagen fibers of an iliac artery (g) without and (h) with an atherosclerotic lesion. (i) CARS (orange) imaging of lipid and TPEF (yellow) imaging of oxidized LDL within foam cells. Images adapted from Wang *et al.* and Le *et al.*

neutralize oxidized LDL into neutral lipid and high density lipoprotein (HDL). Simultaneous CARS imaging of lipid and TPEF imaging of oxidized LDL within foam cells could serve as an indication of foam cell functional activity (Fig. 6(i)). Taken together, combined CARS, SHG, and TPEF imaging demonstrate a powerful capability for compositional analysis of atherosclerotic lesions.[93]

Given such significant advances in optical imaging of atherosclerotic lesions, the future development of multimodal optical endoscopy should hold tremendous promise for clinical diagnosis of cardiovascular diseases. Label-free compositional imaging capability of multimodal NLO microscopy eliminates the need for molecular targeting in complex *in vivo* environment. Additionally, SHG and CARS imaging do not require electronic resonance.[14] Thus, longer wavelength could be used to minimize multiphoton absorption-induced damage to vascular tissues.

A multifunctional endoscope which combines capability for NLO imaging and OCT and IVUS analysis on the same catheter-based platform would enable simultaneous plaque detection, morphology mapping, and composition analysis.[84] Such capability would advance the opportunity for early clinical detection and prevention of atherosclerosis.

6. Lipid-Rich Structures

In addition to obesity-related diseases aforementioned, CARS imaging has also been applied to study myelin sheaths of the central nervous system (CNS).[95] Myelin sheaths are extended membrane of oligodendrocytes in CNS or Schwann cells in peripheral nervous system.[96] Myelin sheaths wrap around axons and facilitate high-speed impulse conduction. Damages to myelin sheaths can be attributed to hereditary neurodegenerative disorders such as leukodystrophies or to acquired diseases such as multiple sclerosis.[97] Currently, demyelinating diseases affect more than two million people worldwide. A typical myelin sheath comprises 70% lipid and 30% protein. Due to such high lipid density, Wang *et al.*[95] successfully imaged intact myelin sheath in live spinal cord tissues using CARS signal arising from CH_2 molecular vibration. Label-free visualization of myelin sheaths further allowed Fu *et al.*[98] to study chemical-induced demyelination of sciatic nerves in real time in living animals. Such capability renders CARS microscopy as a potential, powerful imaging tool for diagnosis and mechanistic studies of myelin diseases.

More recently, CARS microscopy has been applied to study brain structure and pathology.[99,100] CARS signal from brain arises mainly from myelin-rich white matter. Evans *et al.*[99] employed CARS imaging to visualize normal brain structures and glioma in tissue biopsies. Lipid deficient glioma was clearly distinguished from normal brain due to negative and positive CARS contrast, respectively. Thus, the boundary of a brain tumor can be clearly visualized with CARS imaging. Fu *et al.*[100] further employed CARS microscopy for *ex vivo* and *in vivo* imaging of mouse brain. The anatomy of brain axons including myelinated fiber volume, density and orientation was described in detail.[100] Taken together, preliminary applications of CARS microscopy to brain imaging suggest exciting opportunity for future studies of brain connectivity and diseases.

Furthermore, CARS imaging has been applied to visualize significant components of skin structures.[31] Superficial location of skin renders it ideal for optical imaging due to its limited penetration depth. Indeed, Evans *et al.*[31] employed CARS microscopy to image corneocytes, sebaceous glands, and adipocytes at depth of less than 100 μm from the surface of the ear skin in a live mouse. Previous linear optical imaging also showed the capability for sebaceous gland imaging and Raman spectroscopic analysis in human skin.[101] While the function of sebaceous glands is not clearly understood, it is hypothesized to play protective roles including antioxidant and antibacterial.[102] Human diseases relating to sebaceous glands include acne, seborrhea or oily skin, sebaceoma and sebaceous carcinoma or benign and malignant tumors of the sebaceous gland, respectively. Sebaceous glands also transport pheromones and produce lipid, particularly wax ester and squalene.[102] Given the capacity of multiplex CARS imaging for visualization and compositional analysis of lipid structures, it is conceivable that multiplex CARS would be an ideal tool to study the function and diseases of sebaceous glands.[26,27,30]

7. Outlook

The ubiquity of lipid in biological structures and human diseases strongly suggests that CARS microscopy will play a vital role in biological research. Applications of CARS imaging to a wide range of diseases in recent years demonstrated powerful capability of CARS microscopy for diagnosis and mechanistic studies of diseases. However, there are several major drawbacks which might hinder further CARS application. First, a typical CARS microscope set-up is both complex and expensive.[12] The use of multiple laser sources demands builders to have extensive expertise in optics. Moreover, the high cost of pulsed lasers is prohibitive to many research laboratories. As a consequence, CARS microscopy remains accessible to a small number of physical scientists. This drawback limits the discovery of CARS potential and impedes the integration of CARS microscopy into the arsenal of indispensible tools for biologists. Second, limited penetration depth poses significant challenges to clinical application of CARS microscopy.[7] Using near-infrared output of a picosecond laser, synchronously pumped optical parametric oscillator (OPO), for CARS imaging, Ganikhanov *et al.*[103]

achieved a penetration depth of 130 μm. This penetration depth is sufficient for optically accessible organisms or skin imaging, but inadequate for deep tissue imaging of mice or human. This drawback could limit CARS microscopy to laboratory benches for basic science research rather than hospital bedsides for clinical application.

Fortunately, many recent CARS improvements could simplify the set-up, advance its capability, and allow possible clinical application. First, Ganikhanov *et al.* and Evans *et al.* reported the use of OPO CARS where both laser beams came from a single laser source.[31,103] The configuration of OPO CARS eliminates the difficulty commonly associated with synchronization of laser beams coming from two different laser sources. Second, Evans *et al.*[31] employed video-rate OPO CARS with scanning speed of 20 frames per second. Fast scanning rate overcame image distortion arising from respiration motion. Third, Wright *et al.*[104] developed adaptive optics CARS which enhanced CARS signal and increased penetration depth to 260 μm in tissue samples. Most importantly, advances in fiber-delivered CARS and NLO endoscopy strongly suggest an eventual successful development of CARS endoscopy.[105,106] Successful integration of NLO modalities including CARS, SHG, and TPEF with other techniques including OCT on the same catheter-based platform would signal the arrival of optical imaging for clinical diagnosis of diseases.

Acknowledgments

The authors would like to thank professors Ignacio Camarillo, Riyi Shi, and Michael Sturek for the collaborative work on biomedical applications of CARS microscopy. This work is supported by a post-doctoral fellowship F32HL089074 to Le T. T., a NSF grant 0416785-MCB, NIH grants R21 EB004966, and R01 EB007243 to Cheng J. X.

References

1. Calle, E. E. and Kaaks, R., "Overweight, obesity and cancer: Epidemiological evidence and proposed mechanisms," *Nat. Rev. Cancer* **4**(8), 579–591 (2004).
2. Kopelman, P. G., "Obesity as a medical problem," *Nature* **404**, 635–643 (2000).
3. Marx, J., "Unraveling the causes of diabetes," *Science* **296**, 686–689 (2002).
4. Rosen, E. D. and Spiegelman, B. M., "Adipocytes as regulators of energy balance and glucose homeostasis," *Nature* **444**, 847–853 (2006).
5. Ahima, R. S. and Flier, J. S., "Adipose tissue as an endocrine organ," *Trends Endocrinol. Metab.* **11**, 327–332 (2000).
6. Despres, J. P. and Lemieux, I., "Abdominal obesity and metabolic syndrome," *Nature* **444**, 881–887 (2006).
7. Evans, C. L. and Xie, X. S., "Coherent anti-Stokes Raman scattering microscopy: Chemically selective imaging for biology and medicine," *Annu. Rev. Anal. Chem.* **1**, 883–909 (2008).
8. Yeo, G. S., Connie, Hung, C. C., Rochford, J., Keogh, J., Gray, J., Sivaramakrishnan, S., O'Rahilly, S. and Farooqi, I. S., "A *de novo* mutation affecting human TrkB associated with severe obesity and developmental delay," *Nat. Neurosci.* **7**, 1187–1189 (2004).
9. Olden, K. and Wilson, S., "Environmental health and genomics: Visions and implications," *Nat. Rev. Genet.* **1**, 149–153 (2000).
10. Perusse, L. and Bouchard, C., "Role of genetic factors in childhood obesity and in susceptibility to dietary variations," *Ann. Med.* **31**, 19–25 (1999).
11. Fraga, M. F., Ballestar, E., Paz, M. F., Ropero, S., Setien, F., Ballestar, M. L., Heine-Suñer, D., Ciqudosa, J. C., Urioste, M., Benitez, J., Boix-Chornet, M., Sanchez-Aquilera, A., Ling, C., Carlsson, E., Poulsen, P., Vaag, A., Stephan, Z., Spector, T. D., Wu, Y. Z., Plass, C. and Esteller, M., "Epigenetic differences arise during the lifetime of monozygotic twins," *Proc. Natl. Acad. Sci. USA* **102**, 10604–10609 (2005).
12. Cheng, J. X. and Xie, X. S., "Coherent anti-Stokes Raman scattering microscopy: Instrumentation, theory, and applications," *J. Phys. Chem. B* **108**, 827–840 (2004).
13. Cheng, J. X., "Coherent anti-Stokes Raman Scattering microscopy," *Appl. Spectrosc.* **61**, 197–208 (2007).
14. Helmchen, F. and Denk, W., "Deep tissue two-photon microscopy," *Nat. Methods.* **2**, 932–940 (2005).
15. Zipfel, W. R., Williams, R. M., Christie, R., Nikitin, A. Y., Hyman, B. T. and Webb, W. W., "Live tissue intrinsic emission microscopy using multiphoton-excited native fluorescence and second harmonic generation," *Proc. Natl. Acad. Sci. USA* **100**, 7075–7080 (2003).
16. Sturek, M., Alloosh, M., Wenzel, J., Byrd, J. P., Edwards, J. M., Loyd, P. G., Tune, J. D., March, K. L., Miller, M. A., Mokelke, E. A. and Brisbin, I. L. Jr., "Ossabaw island miniature swine: cardiometabolic syndrome assessment," in M. M. Swindle (ed.), *Swine in the Laboratory: Surgery,*

Anesthesia, Imaging, and Experimental Techniques, 2nd edition (CRC Press, Boca Raton, 2007), pp. 397–402.
17. Dyson, M. C., Alloosh, M., Vuchetich, J. P., Mokelke E. A. and Sturek M., "Components of metabolic syndrome and coronary artery disease in female Ossabaw swine fed excess atherogenic diet," *Comp. Med.* **56**, 35–45 (2006).
18. Rosen, E. D. and MacDougald, O. A., "Adipocyte differentiation from the inside out," *Nat. Rev. Mol. Cell. Biol.* **7**, 885–896 (2006).
19. Green, H. and Kehinde, O., "Sublines of mouse 3T3 cells that accumulate lipid," *Cell* **1**, 113–116 (1974).
20. Lee, Y. H., Chen, S. Y., Wiesner, R. J. and Huang, Y. F., "Simple flow cytometric method used to assess lipid accumulation in fat cells," *J. Lipid. Res.* **45**, 1162–1167 (2004).
21. Nan, X. L., Cheng, J. X. and Xie, X. S., "Vibrational imaging of lipid droplets in live fibroblast cells with coherent anti-Stokes Raman scattering microscopy," *J. Lipid. Res.* **44**, 2202–2208 (2003).
22. Nan, X. L., Potma, E. O. and Xie, X. S., "Nonperturbative chemical imaging of organelle transport in living cells with coherent anti-stokes Raman scattering microscopy," *Biophys. J.* **91**, 728–735 (2006).
23. Yamaguchi, T., Omatsu, N., Morimoto, E., Nakashima, H., Ueno, K., Tanaka, T., Satouchi, K., Hirose, F. and Osumi, T., "CGI-58 facilitates lipolysis on lipid droplets but is not involved in the vesiculation of lipid droplets caused by hormonal stimulation," *J. Lipid. Res.* **48**, 1078–1089 (2007).
24. Fujimoto, T., Ohsaki, Y., Cheng, J., Suzuki, M. and Shinohara, Y., "Lipid droplets: A classic organelle with new outfits," *Histochem. Cell Biol.* **130**, 263–279 (2008).
25. Debarre, D., Supato, W., Pena, A. M., Fabre, A., Tordjmann, T., Combettes, L., Schanne-Klein, M. C. and Beaurepaire, E., "Imaging lipid bodies in cells and tissues using third-harmonic generation microscopy," *Nat. Methods* **3**, 47–53 (2006).
26. Cheng, J. X., Volkmer, A., Book, L. D. and Xie, X. S., "Multiplex coherent anti-Stokes Raman scattering microspectroscopy and study of lipid vesicles," *J. Phys. Chem. B* **106**, 8493–8498 (2002).
27. Muller, M. and Schins, J. M., "Imaging the thermodynamic state of lipid membranes with multiplex CARS microscopy," *J. Phys. Chem. B* **106**, 3715–3723 (2002).
28. Li, L., Wang, H. F. and Cheng, J. X., "Quantitative coherent anti-Stokes Raman scattering imaging of lipid distribution in coexisting domains," *Biophys. J.* **89**, 3480–3490 (2005).
29. Burkacky, O., Zumbusch, A., Brackmann, C. and Enejder, A., "Dual-pump coherent anti-Stokes-Raman scattering microscopy," *Opt. Lett.* **31**, 3656–3658 (2006).
30. Rinia, H. A., Burger, K. N. J., Bonn, M. and Muller, M., "Quantitative label-free imaging of lipid composition and packing of individual cellular lipid droplets using multiplex CARS microscopy," *Biophys. J.* **95**, 4908–4918 (2008).
31. Evans, C. L., Potma, E. O., Pouris'haag, M., Côté, D., Lin, P. C. and Xie, X. S., "Chemical imaging of tissue *in vivo* with video-rate coherent anti-Stokes Raman scattering microscopy," *Proc. Natl. Acad. Sci. USA* **102**, 16807–16812 (2005).
32. Huff, T. B. and Cheng, J. X., "*In vivo* coherent anti-Stokes Raman scattering imaging of sciatic nerve tissue," *J. Microsc.* **225**, 175–182 (2007).
33. Guo, Y., Walther, T. C., Rao, M., Stuurman, N., Goshima, G., Terayama, K., Wong, J. S., Vale, R. D., Walter, P. and Farese, R. V., "Functional genomic screen reveals genes involved in lipid-droplet formation and utilization," *Nature* **453**, 657–661 (2008).
34. Zhang, J., Campbell, R. E., Ting, A. Y. and Tsien, R. Y., "Creating new fluorescent probes for cell biology," *Nat. Rev. Mol. Cell. Biol.* **3**, 906–918 (2002).
35. Shaner, N. C., Steinbach, P. A. and Tsien, R. Y., "A guide to choosing fluorescent proteins," *Nat. Methods* **2**, 905–909 (2005).
36. Yao, J., Munson, K. M., Webb, W. W. and Lis, J. T., "Dynamics of heat shock factor association with native gene loci in living cells," *Nature* **442**, 1050–1053 (2006).
37. Le, T. T., Harlepp, S., Guet, C. C., Dittmar, K., Emonet, T., Pan, T. and Cluzel, P., "Real-time RNA profiling within a single bacterium," *Proc. Natl. Acad. Sci. USA* **102**, 9160–9164 (2005).
38. Jares-Erijman, E. A. and Jovin, T. M., "FRET imaging," *Nat. Biotechnol.* **21**, 1387–1395 (2003).
39. Haustein, E. and Schwille, P., "Fluorescence correlation spectroscopy: Novel variations of an established technique," *Annu. Rev. Biophys. Biomol. Struct.* **36**, 151–169 (2007).
40. Martin, S. and Parton, R. G., "Lipid droplets: A unified view of a dynamic organelle," *Nat. Rev. Mol. Cell. Biol.* **7**, 373–378 (2006).
41. Fukumura, D. *et al.*, "Paracrine regulation of angiogenesis and adipocyte differentiation during *in vivo* adipogenesis," *Circ. Res.* **93**, 88–97 (2003).
42. Brown, E. B., Campbell, R. B., Tsuzuki, Y., Xu, L., Carmeliet, P., Fukumura, D. and Jain, R. K., "*In vivo* measurement of gene expression, angiogenesis and physiological function in tumors using multiphoton laser scanning microscopy," *Nat. Med.* **7**, 864–868 (2001).
43. Alexandrakis, G., Brown, E. B., Tang, R. T., Mckee, T. D., Campbell, R. B., Boucher, Y. and Jain R. K., "Two-photon fluorescence correlation microscopy reveals the two-phase nature

of transport in tumors," *Nat. Med.* **10**, 203–207 (2004).
44. Kadereit, B., Kumar, P., Wang, W. J., Miranda, D., Snapp, E. L., Severina, N., Torregroza, I., Evans, T. and Silver, D. L., "Evolutionarily conserved gene family important for fat storage," *Proc. Natl. Acad. Sci. USA* **105**, 94–99 (2008).
45. Kaletta, T. and Hengartner, M. O., "Finding function in novel targets: *C-elegans* as a model organism," *Nat. Rev. Drug Discovery* **5**, 387–398 (2006).
46. Reinke, V. and White, K. P., "Developmental genomic approaches in model organisms," *Annu. Rev. Genomics Hum. Genet.* **3**, 153–178 (2002).
47. Zon, L. I. and Peterson, R. T., "*In vivo* drug discovery in the zebrafish," *Nat. Rev. Drug Discovery* **4**, 35–44 (2005).
48. Stoletov, K., Montel, V., Lester, R. D., Gonias, S. L. and Klemke, R., "High-resolution imaging of the dynamic tumor cell-vascular interface in transparent zebrafish," *Proc. Natl. Acad. Sci. USA* **104**, 17406–17411 (2007).
49. Hellerer, T., Aẍang, C., Brackmann, C., Hillertz, P., Pilon, M. and Enejder, A., "Monitoring of lipid storage in *Caenorhabditis elegans* using coherent anti-Stokes Raman scattering (CARS) microscopy," *Proc. Natl. Acad. Sci. USA* **104**, 14658–14663 (2007).
50. Lorincz, A. M. and Sukumar, S., Molecular links between obesity and breast cancer," *Endocr. Relat. Cancer.* **13**, 279–292 (2006).
51. Iyengar, P., Combs, T. P., Shah, S. J., Gauon-Evans, V., Pollard, J. W., Albanese, C., Flanagan, L., Tenniswood, M. P., Guha, C., Lisanti, M. P., Pestell, R. G. and Scherer, P. E., "Adipocyte-secreted factors synergistically promote mammary tumorigenesis through induction of anti-apoptotic transcriptional programs and proto-oncogene stabilization," *Oncogene* **22**, 6408–6423 (2003).
52. Hanahan, D. and Weinberg, R. A., "The hallmarks of cancer," *Cell* **100**, 57–70 (2000).
53. Bissell, M. J. and Radisky, D., "Putting tumours in context," *Nat. Rev. Cancer* **1**, 46–54 (2001).
54. Tlsty, T. D. and Coussens, L. M., "Tumor stroma and regulation of cancer development," *Annu. Rev. Pathol. Mech. Dis.* **1**, 119–150 (2006).
55. Kalluri, R. and Zeisberg, M., "Fibroblasts in cancer," *Nat. Rev. Cancer* **6**, 392–401 (2006).
56. Karnoub, A. E., Dash, A. B., Vo, A. P., Sullivan, A., Brooks, M. W., Richardson, A. L., Polyak, K., Tubo, R. and Weinberg, R. A., "Mesenchymal stem cells within tumour stroma promote breast cancer metastasis," *Nature* **449**, 557–563 (2007).
57. Wyckoff, J. B., Wang, Y., Lin, E. Y., Li, Y. F., Goswami, S., Stanley, E. R., Segall, J. E., Pollard, J. W. and Candeelis, J., "Direct visualization of macrophage-assisted tumor cell intravasation in mammary tumors," *Cancer Res.* **67**, 2649–2656 (2007).
58. Provenzano, P. P., Eliceiri, K. W., Campbell, J. M., Inman, D. R., White, J. G. and Keely, P. J., "Collagen reorganization at the tumor-stromal interface facilitates local invasion," *BMC Med.* **4**, 38 (2006).
59. Jain, R. K., di Tomaso, E., Duda, D. G., Loeffler, J. S., Sorensen, A. G. and Batchelor, T. T., "Angiogenesis in brain tumours," *Nat. Rev. Neurosci.* **8**, 610–622 (2007).
60. Fukumura, D., Xavier, R., Sugiura, T., Chen, Y., Park, E. C., Lu, N., Selig, M., Nielsen, G., Taksir, T., Jain, R. K. and Seed, B., "Tumor induction of VEGF promoter activity in stromal cells," *Cell* **94**, 715–725 (1998).
61. Le, T. T., Rehrer, C. W., Huff, T. B., Nichols, M. B., Camarillo, I. G. and Chen, J. X., "Nonlinear optical imaging to evaluate the impact of obesity on mammary gland and tumor stroma," *Mol. Imaging* **6**, 205–211 (2007).
62. Thordarson, G., Lee, A. V., McCarty, M., Van Horn, K., Chu, O., Chou, Y. C., Yang, J., Guzman, R. C., Nandi, S. and Talamantes, F., "Growth and characterization of *N*-methyl-*N*-nitrosourea-induced mammary tumors in intact and ovariectomized rats," *Carcinogenesis* **22**, 2039–2048 (2001).
63. Provenzano, P. P., Inman, D. R., Eliceiri, K. W., Knittel, J. G., Yan, L., Rueden, C. T., White, J. G. and Keely, P. J., "Collagen density promotes mammary tumor initiation and progression," *BMC Med.* **6**, 11 (2008).
64. Fouser, L., Iruelaarispe, L., Bornstein, P. and Sage, E. H., "Transcriptional activity of the α-1(I)-collagen promoter is correlated with the formation of capillary-like structures by endothelial cells *in vitro*," *J. Biol. Chem.* **266**, 18345–18351 (1991).
65. Ahmed, F., Wyckoff, J., Lin, E. Y., Wang, W., Wing, Y., Hennighausen, L., Miyazaki, J., Jones, J., Pollard, J. W., Condeelis, J. S. and Segall, J. E., "GFP expression in the mammary gland for imaging of mammary tumor cells in transgenic mice," *Cancer Res.* **62**, 7166–7169 (2002).
66. Dailey, M. E. and Waite, M., "Confocal imaging of microglial cell dynamics in hippocampal slice cultures," *Methods* **18**, 222–230 (1999).
67. Shoelson, S. E., Herrero, L. and Naaz, A., "Obesity, inflammation, and insulin resistance," *Gastroenterology* **132**, 2169–2180 (2007).
68. Rose, D. P., Connolly, J. M. and Meschte, C. L., "Effect of dietary fat on human breast cancer growth and lung metastasis in nude mice," *J. Natl. Cancer Inst.* **83**, 1491–1495 (1991).
69. Risch, H. A., Jain, M., Marrett, L. D. and Howe, G. R., "Dietary fat intake and risk of epithelial

ovarian cancer," *J. Natl. Cancer Inst.* **86**, 1409–1415 (1994).
70. Garofalo, C. and Surmacz, E., "Leptin and cancer," *J. Cell Physiol.* **207**, 12–22 (2006).
71. Ramos, C. V. and Taylor, H. B., "Lipid-rich carcinoma of the breast: A clinicopathologic analysis of 13 examples," *Cancer* **33**, 812–819 (1973).
72. Metser, U. *et al.,* "F-18-FDG PET/CT in the evaluation of adrenal masses," *J. Nucl. Med.* **47**, 32–37 (2006).
73. Sijens, P. E., Levendag, P. C., Vecht, C. J., vanDijk, P. and Oudkerk, M., "H-1 MR spectroscopy detection of lipids and lactate in metastatic brain tumors," *NMR Biomed.* **9**, 65–71 (1996).
74. Pierce, M. C., Javier, D. J. and Richards-Kortum, R., "Optical contrast agents and imaging systems for detection and diagnosis of cancer," *Int. J. Cancer* **123**, 1979–1990 (2008).
75. Tearney, G. J., Brezinski, M. E., Bouma, B. E., Boppart, S. A., Pitris, C., Southern, J. F. and Fujimoto, J. G., "*In vivo* endoscopic optical biopsy with optical coherence tomography," *Science* **276**, 2037–2039 (1997).
76. Tromberg, B. J., Pogue, B. W., Paulsen, K. D., Yodh, A. G., Boas, D. A. and Cerussi, A. E., "Assessing the future of diffuse optical imaging technologies for breast cancer management," *Med. Phys.* **35**, 2443–2451 (2008).
77. Rosemond, W., Flegal, K., Furie, K., Go, A., Greenlund, K., Haase, N., Hailpern, S. M., Ho, M., Howard, V., Kissela, B., Kittner, S., Lloyd-Jones, D., McDermott, M., Meigs, J., Moy, C., Nickol, G., O'Donell, C., Roger, V., Sorlie, P., Steinberger, J., Thom, T., Wilson, M. and Hang, Y., "Heart disease and strokes statistic — 2008 update," *Circulation* **117**, 25–146 (2008).
78. Libby, P. and Aikawa, M., "Stabilization of atherosclerotic plaques: New mechanisms and clinical targets," *Nat. Med.* **8**, 1257–1262 (2002).
79. Tuzcu, E. M., Kapadia, S. R., Tutar, E., Ziada, K. M., Hobbs, R. E., McCarthy, P. M., Young, J. B. and Nissen, S. E., "High prevalence of coronary atherosclerosis in asymptomatic teenagers and young adults — Evidence from intravascular ultrasound," *Circulation* **103**, 2705–2710 (2001).
80. Virmani, R., Kolodgie, F., Burke, A. P., Farb, A. and Schwartz, S. M., "Lessons from sudden coronary death — A comprehensive morphological classification scheme for atherosclerotic lesions," *Arterioscler. Thromb. Vasc. Biol.* **20**, 1262–1275 (2000).
81. Steinberg, D., "Atherogenesis in perspective: Hypercholesterolemia and inflammation as partners in crime," *Nature Med.* **8**, 1211–1217 (2002).
82. Lusis, A. J., "Atherosclerosis," *Nature* **407**, 233–241 (2000).
83. Davies, M. J., Richardson, P. D., Woolf, N., Katz, D. R. and Mann, J., "Risk of thrombosis in human atherosclerotic plaques — role of extracellular lipid, macrophage, and smooth-muscle cell content," *Br. Heart. J.* **69**, 377–381 (1993).
84. Choudhury, R. P., Fuster, V. and Fayad, Z. A., "Molecular, cellular and functional imaging of atherothrombosis," *Nat. Rev. Drug. Discov.* **3**, 913–925 (2004).
85. Marcu, L., Fishbein, M. C., Maarek, J. M. I. and Grundfest, W. S., "Discrimination of human coronary artery atherosclerotic lipid-rich lesions by time-resolved laser-induced fluorescence spectroscopy," *Arterioscler. Thromb. Vasc. Biol.* **21**, 1244–1250 (2001).
86. Motz, J. T., Fitzmaurice, M., Miller, A., Gandhi, S. J., Haka, A. S., Galindo, L. H., Dasari, R. R., Kramer, J. R. and Feld, M. S., "*In vivo* Raman spectral pathology of human atherosclerosis and vulnerable plaque," *J. Biomed. Opt.* **11**, 021003 (2006).
87. Nadkarni, S. K., Bouma, B., Helg, T., Chan, R., Halpern, E., Chau, A., Minsky, M. S., Motz, J. T., Houser, S. L. and Tearney, G. J., "Characterization of atherosclerotic plaques by laser speckle imaging," *Circulation* **112**, 885–892 (2005).
88. Eriksson, E. E., Xie, X., Werr, J., Thoren, P. and Lindbom, L., "Direct viewing of atherosclerosis in vivo: plaque invasion by leukocytes is initiated by the endothelial selectins," *FASEB J.* **15**, 1149–1157 (2001).
89. Huo, Y. Q., Schober, A., Forlow, S. B., Smith, D. F., Hyman, M. C., Jung, S., Littman, D. R., Weber, C. and Ley, K., "Circulating activated platelets exacerbate atherosclerosis in mice deficient in apolipoprotein E," *Nature Med.* **9**, 61–67 (2003).
90. Zoumi, A., Lu, X. A., Kassab, G. S. and Tromberg, B. J., "Imaging coronary artery microstructure using second-harmonic and two-photon fluorescence microscopy," *Biophys. J.* **87**, 2778–2786 (2004).
91. Yu, W. M., Braz, J. C., Dutton, A. M., Prusakov, P. and Rekhter, M., "*In vivo* imaging of atherosclerotic plaques in apolipoprotein E deficient mice using nonlinear microscopy," *J. Biomed. Opt.* **12**, 054008 (2007).
92. van Zandvoort, M., Engels, W., Douma, K., Beckers, L., Oude Egbrink, M., Daemen, M. and Slaaf, D. W., "Two-photon microscopy for imaging of the (atherosclerotic) vascular wall: A proof of concept study," *J. Vasc. Res.* **41**, 54–63 (2004).
93. Le, T. T., Langohr, I. M., Locker, M. J., Sturek, M. and Cheng, J. X., "Label-free molecular imaging of atherosclerotic lesions using multimodal nonlinear

optical microscopy," *J. Biomed. Opt.* **12**, 054007 (2007).
94. Wang, H. W., Le, T. T. and Cheng, J. X., "Label-free imaging of arterial cells and extracellular matrix using a multimodal CARS microscope," *Opt. Comm.* **281**, 1813–1822 (2008).
95. Wang, H. F., Fu, Y., Zickmund, P., Shi, R. Y. and Cheng, J. X., "Coherent anti-stokes Raman scattering imaging of axonal myelin in live spinal tissues," *Biophys. J.* **89**, 581–591 (2005).
96. Sherman, D. L. and Brophy, P. J., "Mechanisms of axon ensheathment and myelin growth," *Nat. Rev. Neurosci.* **6**, 683–690 (2005).
97. Sospedra, M. and Martin, R., "Immunology of multiple sclerosis," *Annu. Rev. Immunol.* **23**, 683–747 (2005).
98. Fu, Y., Wang, H. F., Huff, T. B., Shi, R. and Cheng, J. X., "Coherent anti-stokes Raman scattering imaging of myelin degradation reveals a calcium-dependent pathway in lyso-PtdCho-induced demyelination," *J. Neurosci. Res.* **85**, 2870–2881 (2007).
99. Evans, C. L., Xu, X., Kesari, S., Xie, X. S., Wong, S. T. C. and Young. G. S., "Chemically selective imaging of brain structures with CARS microscopy," *Opt. Express.* **15**, 12076–12087 (2007).
100. Fu, Y., Huff, T. B., Wang, H. W., Wang, H. F. and Cheng, J. X., "*Ex vivo* and *in vivo* imaging of myelin fibers in mouse brain by coherent anti-Stokes Raman microscopy," *Opt. Express.* **16**, 19396–19409 (2008).
101. Caspers, P. J., Lucassen, G. W. and Puppels, G. J., "Combined in vivo confocal Raman spectroscopy and confocal microscopy of human skin," *Biophys. J.* **85**, 572–580 (2003).
102. Smith, K. R. and Thiboutot, D. M., "Sebaceous gland lipids: Friend or foe?," *J. Lipid. Res.* **49**, 271–281 (2008).
103. Ganikhanov, F., Carrasco, S., Xie, X. S., Katz, M., Seitz, W. and Kopf, D., "Broadly tunable dual-wavelength light source for coherent anti-Stokes Raman scattering microscopy," *Opt. Lett.* **31**, 1292–1294 (2006).
104. Wright, A. J., Poland, S. P., Girkin, J. M., Freudiger, C. W., Evans, C. L. and Xie, X. S., "Adaptive optics for enhanced signal in CARS microscopy," *Opt. Express.* **15**, 18209–18219 (2007).
105. Legare, F., Evans, C. L., Ganikhanov, F. and Xie, X. S., "Towards CARS endoscopy," *Opt. Express.* **14**, 4427–4432 (2006).
106. Llewellyn, M. E., Barretto, R. P. J., Delp, S. L. and Schnitzer, M. J., "Minimally invasive high-speed imaging of sarcomere contractile dynamics in mice and humans," *Nature* **454**, 784–788 (2008).